EUROPEAN ORGANIZATION FOR NUCLEAR RESEARCH
CERN - PS DIVISION

CTF3 Note 052 (MD)
PS/AE Note 2002-194
(Preliminary Phase)

Report on the Second Operation Period of the CTF3 Preliminary Phase in 2002, 27 May - 23 August

R. Corsini, L. Rinolfi, F. Tecker, CERN, Geneva

A. Ferrari (Ed.), Department of Radiation Sciences, Uppsala University

P. Royer, Institut de Physique des Hautes Energies, Université de Lausanne

Abstract

In this note, we report on the first demonstration of the bunch combination scheme in the CTF3 Preliminary Phase. We describe the procedures that were followed to combine at first two bunch trains at about half the nominal energy, and then to multiply the bunch frequency by four and five at the nominal energy (350 MeV). We also report on the other measurements which were performed during the summer 2002.

Geneva, Switzerland
November 13, 2002

1 Goals

The main goal for this second operation period of 2002 was to demonstrate the bunch combination scheme [1], after installation of the CERN RF deflectors in the ring. During the first week of this operation period, we managed to combine two bunch trains, however with a beam energy half the nominal one. Bunch combination factors of four and five were obtained in the nominal conditions during the second week of operation. Then, during the summer, other measurements were made to improve our understanding of the optics in the linac, the injection line and the ring.

2 Installation and test of the CERN RF deflectors

The installation of the CERN RF deflectors HR.SDH71 and HR.SDH91 in the EPA ring was made between May 24 and May 27, 2002. No vacuum leak was detected, the connection to the water system at 30°C worked well and the modulator WL.MDK33, which powers the RF deflectors, was implemented.

During the first week of operation, the RF deflectors were not properly mounted: the RF wave was travelling in the same direction as the electrons, instead of travelling against the beam, as required by the negative group velocity in the structure. The RF wave was therefore not resonant with the beam. However, due to the short length of the RF deflectors, a residual kick, much weaker than the expected one, was given to the beam. Therefore, we could start using the RF deflectors while preparing the RF network modifications. After having connected the input waveguide to the downstream port of the RF deflectors, HR.SDH71 and HR.SDH91 were working properly.

3 First combination of two bunch trains

As explained in the previous section, the kick given by the RF deflectors was initially much too weak to inject properly with the RF deflectors only. However, it was possible to inject at the nominal energy using the fast kicker in conjunction with HR.SDH91. Such a scheme did not allow combination but proved the RF injection. We managed to perform a first combination by decreasing the beam energy to about half the nominal one and using the bumpers to bring the closed orbit nearer to the injection septum.

In these conditions, we injected two successive pulses from the gun and observed the synchrotron light emitted in the bending magnet HR.BHZ56, with the streak camera: the first combination of two bunch trains in the EPA ring was successfully performed, as shown in Figure 1.

4 Bunch frequency multiplication with a factor four

After having properly mounted the RF deflectors, the bunch frequency multiplication with a factor four could be performed in the nominal conditions, on June 18. The charge per bunch was about 0.08 nC in the linac and the frequency was set to 2.998550 GHz.

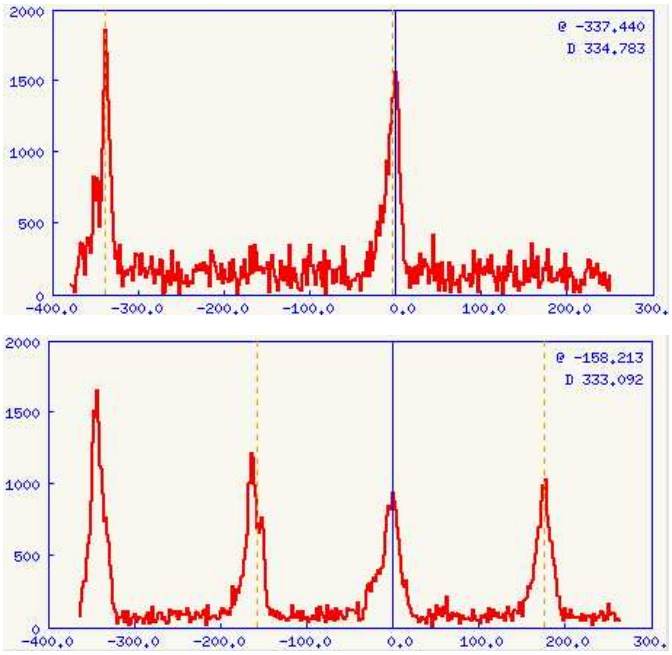

Figure 1: Longitudinal intensity profile of the electron pulses measured by the streak camera. The upper graph shows two successive bunches of the first pulse spaced by 333 ps at the first turn. The lower graph shows the bunches after combination. The bunches of the second train are interleaved with the ones of the first train (at about halfway).

The RF pulse on WL.MDK33 (which feeds the RF deflectors) was shortened such that the field in HR.SDH91 was only present during the injection of the pulse and that there was no field in HR.SDH71 when the bunches arrived there after one turn in the ring. In addition, the attenuation of HR.SDH71 was set to the maximum value, to be sure that the beam does not receive any kick in that RF deflector. Then, we adjusted the phase of HR.SDH91 such that the beam receives the largest possible kick when passing through this RF deflector (the beam position monitor HR.UMA91 was used in order to monitor the position of the beam just downstream of HR.SDH91). The settings of the injection septum HIE.SMH33, of the power of modulator WL.MDK33, and of the correction magnets in the injection line were adjusted in order to properly inject one electron pulse into the EPA ring and to have it circulate during at least four turns without significant losses.

Afterwards, the length of the RF pulse was increased in order to produce a kicks in both HR.SDH71 and HR.SDH91 at the following turns. The attenuator of HR.SDH71 was set to its minimum value, such that the kick has the same amplitude in both RF deflectors. The phase of HR.SDH71 was adjusted such that the pulse does not receive any kick when going through this RF deflector at the second turn, i.e. that it arrives in HR.SDH71 at the zero-crossing of the deflecting field. This also ensures that the pulse receives a maximum ”negative” kick at the third turn, i.e. in the opposite direction as compared to the first turn. Then, four pulses were injected into the ring instead of one, and we could indeed check that the signal measured in HR.UMA83 was increasing almost linearly turn after turn: the charge in the pulse was about four times larger at the fourth turn than at the first one (see Figure 2). Finally, streak camera images of the pulse structure allowed us to directly observe the bunch train combination with a factor four, as shown in Figures 3 and 4.

Figure 2: Visualization of the signal from the beam position monitor HR.UMA83 (bottom) turn after turn while the bunch train combination is performed. The RF pulse in WL.MDK33 is also shown (top).

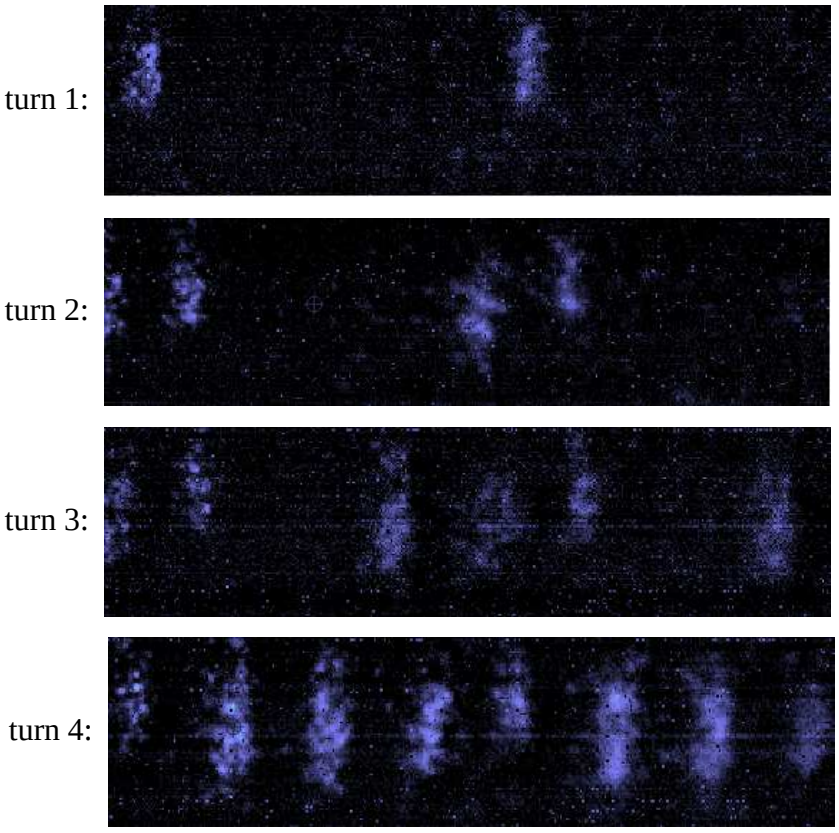

Figure 3: Streak camera images of the electron pulse in the EPA ring while the bunch frequency multiplication is performed: on the upper image, one can see two successive bunches of one pulse at turn 1. The following images show bunches of two pulses at turn 2, three pulses at turn 3 and four pulses at turn 4 (from top to bottom).

turn 1:

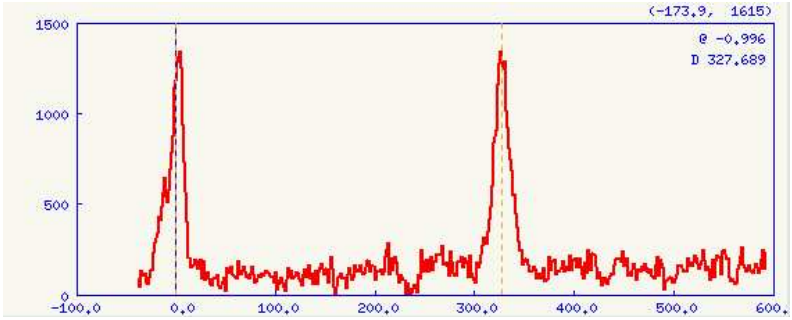

turn 2:

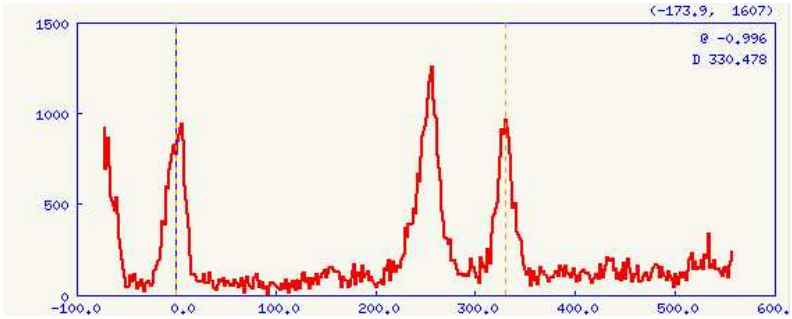

turn 3:

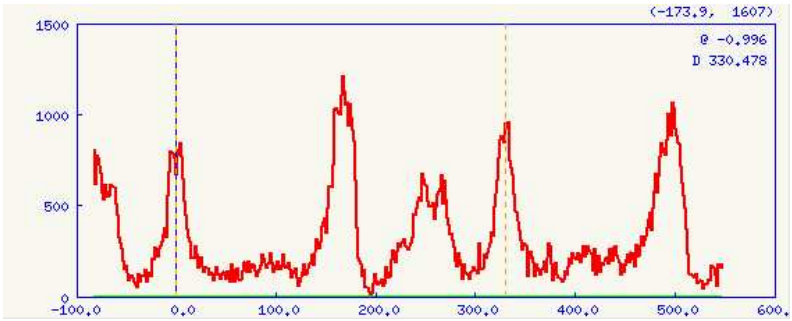

turn 4:

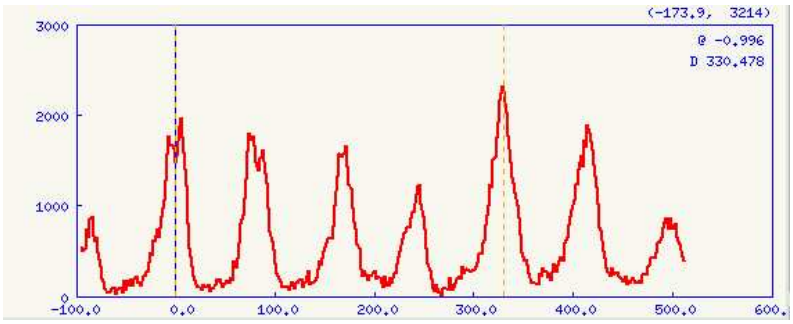

Figure 4: Longitudinal intensity profiles for the same sequence as in Figure 3. The horizontal axis is in ps. The bunch spacing is about 83 ps.

5 Bunch frequency multiplication with a factor five

After having successfully performed the bunch train combination with a factor four, we managed to combine five electron pulses in the EPA ring on June 21.

In order to change the combination factor from four to five, a change of the RF frequency is necessary.

Let λ_0 be the nominal RF wavelength (corresponding to a frequency $f_0 = 2.998550\,\mathrm{GHz}$), one must have [1]:

$$C = n\lambda_0 \pm \lambda_0/N,$$

where C is the ring circumference, n is an integer and N is the combination factor.

The bunch train combination with a factor $N = 4$ was obtained with $f_0 = 2.998550\,\mathrm{GHz}$. From the approximate ring circumference (125.65 m), we know that in our case $n = 1257$ and that one has a minus sign in the previous equation. Let λ_5 be the RF wavelength for a bunch train combination with a factor five, then one has:

$$\lambda_5 = \lambda_0 \times \frac{n - 1/4}{n - 1/5} = 0.099975165\,\mathrm{m}$$

and the new RF frequency must therefore be $f_5 = 2.998669\,\mathrm{GHz}$.

When changing the operating frequency, a temperature decrease by 2°C was also necessary in the bunching system, the accelerating structures and the RF deflectors, in order to change the resonant frequency of these cavities.

After having changed the RF frequency and the temperature, we optimized the machine optics and the settings of the RF deflectors in order to properly inject one electron pulse into the ring and to have it circulate over five turns. Next, five electron pulses were injected into the EPA ring instead of one. Streak camera images were recorded and analyzed: they show a successful bunch train combination with a factor five. Figure 5 shows the structure of the pulse after the bunch frequency multiplication: there are indeed five bunches within 333 ps.

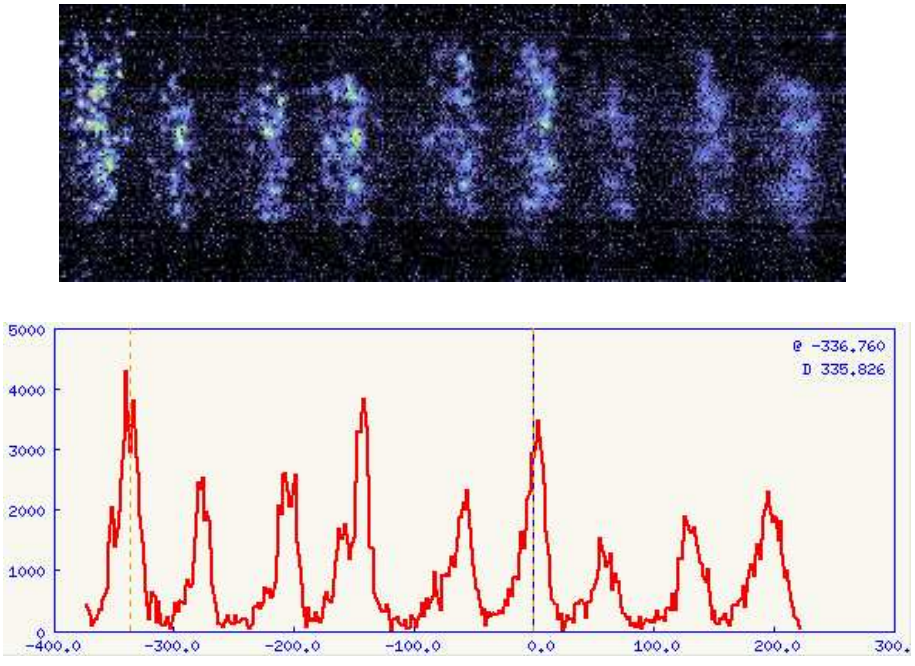

Figure 5: Streak camera image (top) and longitudinal profile (bottom) of the electron pulse after performing the bunch combination with a factor five. The bunch spacing is now about 66 ps.

6 Other measurements

During the summer 2002, several measurements were performed in order to understand better the optics of the CTF3 machine and to further improve its performances.

6.1 Optimization of the injection with the RF deflector

After having successfully performed the bunch train combination, we tried to improve the injection efficiency with the RF deflector HR.SDH91. For this purpose, we studied in details the optics at the end of the linac and in the injection line.

In the linac, after having improved the alignment of the beam along its path, a quadrupole scan was performed in order to measure the Twiss parameters at the entrance of the matching section. The results that were obtained are summarized in Table 1. No significant difference was observed when compared to previous measurements [2, 3]. Assuming a beam energy of 332 MeV, we recalculated the values of the currents for the five quadrupoles of the matching section, in order to have the nominal Twiss parameters at the entrance of the injection line. We found 115.9 A in WL.QNF351, 95.0 A in WL.QNF352, 18.7 A in WL.QNF353, 135.0 A in WL.QNF371, and 180.8 A in WL.QNF372.

Lattice function	Measured value
β_x (m)	11.40
α_x	-0.43
ϵ_x (mm.mrad)	15.2
β_y (m)	43.36
α_y	-6.27
ϵ_y (mm.mrad)	15.2

Table 1: Twiss parameters and normalised rms emittance at the entrance of WL.QNF351, as derived from a quadrupole scan in WL.WBS37.

In the injection line, a vertical correcting dipole HIE.DVT23 was installed such that there is a phase advance close to $\pi/2$ between HIE.DVT23 and the dipole magnet HIE.BVT30. Also, the horizontal correcting dipole HIE.DHZ25 was displaced in order to have a phase advance of about $\pi/2$ between HIE.DHZ25 and the injection septum HIE.SMH33. Both HIE.DVT23 and HIE.DHZ25 can be used to optimize the beam path along the injection line. Furthermore, after having moved the vacuum gauges further away from the beam pipe, we managed to suppress the parasitic vertical kick given by their magnetic field at the entrance of HI.BSH00. Finally, we noticed that, with the nominal settings of the quadrupoles in the injection line, we do not manage to properly inject the beam in EPA. By changing the current in HIE.QDW24 from 90 to 95 A, we can correct for these effects: the transmission between the injection line and the ring becomes very good, and we also obtain the expected beam shape in HIE.MTV30. However, with these new settings, MAD simulations predict a very large vertical β-function, as well as a non-zero vertical dispersion, which we do not observe in reality. This discrepancy between the experimental and theoretical settings of HIE.QDW24 is observed in dispersion measurements as well, see section 6.3.

For the first combination studies, the currents in HR.BHZ and in the quadrupoles were adjusted empirically to obtain a good transmission over a few turns in the ring. However, we noticed that, according to MAD simulations, these settings do not lead to a zero-dispersion in the EPA long straight lines. Probably, this ring optics gave a better match to the transfer line, which had not been completely optimized at that time.

After reoptimization of the injection line, we tuned the optics of the ring such that the MAD model gives a small dispersion in the EPA long straight lines. A comparison of the settings for HR.BHZ and the quadrupoles of the ring is given in Table 2. The corresponding dispersion curves, calculated with MAD, are given in Figures 6 and 7.

Element of the ring	Current (A)	
	21 June	9 July
HR.BHZ	294.02	291.32
HR.QFWA	31.51	31.46
HR.QFWB	17.89	17.81
HR.QFLA	92.76	92.39
HR.QFLB	11.52	11.03
HR.QFI	19.01	19.12
HR.QFN	22.34	22.23
HR.QDN	22.40	22.33
HR.QTRA	6.90	6.87
HR.QTRB	41.61	42.61

Table 2: Comparison of the settings for the isochronous ring: the first column corresponds to the settings of June 21 (first bunch train combination with a factor five) and the second column corresponds to the settings of July 9, after optimization of the ring optics. Note that the energy may have been slightly different at these two dates.

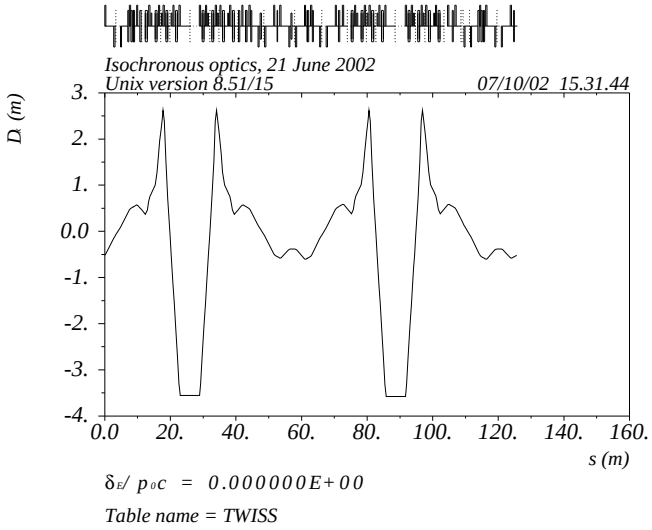

Figure 6: Dispersion curve in the EPA ring with the settings of June 21, when the first bunch train combination with a factor five was performed.

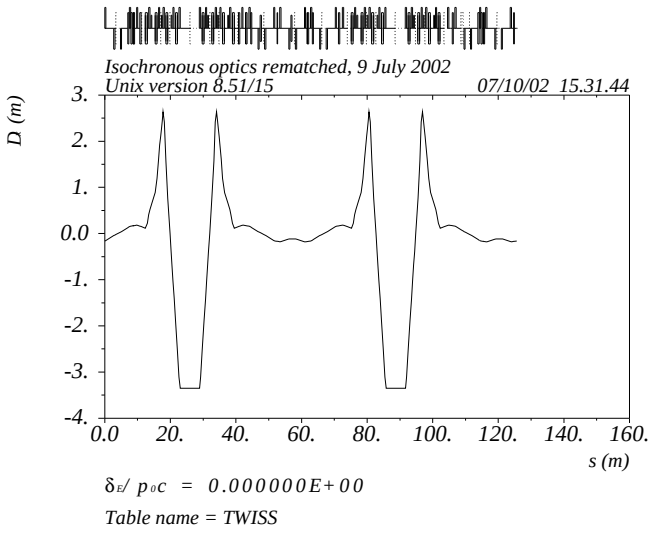

Figure 7: Dispersion curve in the EPA ring with the settings of July 9, after optimization of the isochronous optics.

After this optimization, it was possible to inject the beam into the ring, with either the fast kickers or the RF deflectors, and to make it circulate over several turns without significant losses, see Figure 8.

Figure 8: Signal recorded in the beam position monitor HR.UMA83. On the left-hand side, the electron pulse is injected with the fast kicker. On the right-hand side, the RF deflector HR.SDH91 is used for the injection. In both cases, the beam is ejected after six turns by the extraction kicker. The apparent delay between the signals results from different cable lengths, the RF pulse shown in green actually arrives in the RF deflector at the same time as the injected electron pulse.

6.2 Dispersion measurements in the HIE line and the ring injection region

Dispersion measurements were performed along the HIE line and at the ring entrance just after the injection septum. For this purpose, we have used three cameras (HIE.MTV01, HIE.MTV23, and HIE.MTV30), five beam position monitors (HIE.UMA21, HIE.UMA22, and

HIE.UMA23 in the injection line, HR.UMA83 and HR.UMA91 in the ring), and one SEM-Grid (HIE.MSH23). The currents in all magnetic elements were changed in order to simulate relative energy variations, while the corresponding beam positions were recorded in each of the diagnostic tools. Figure 9 shows the measured values of the horizontal and vertical dispersions.

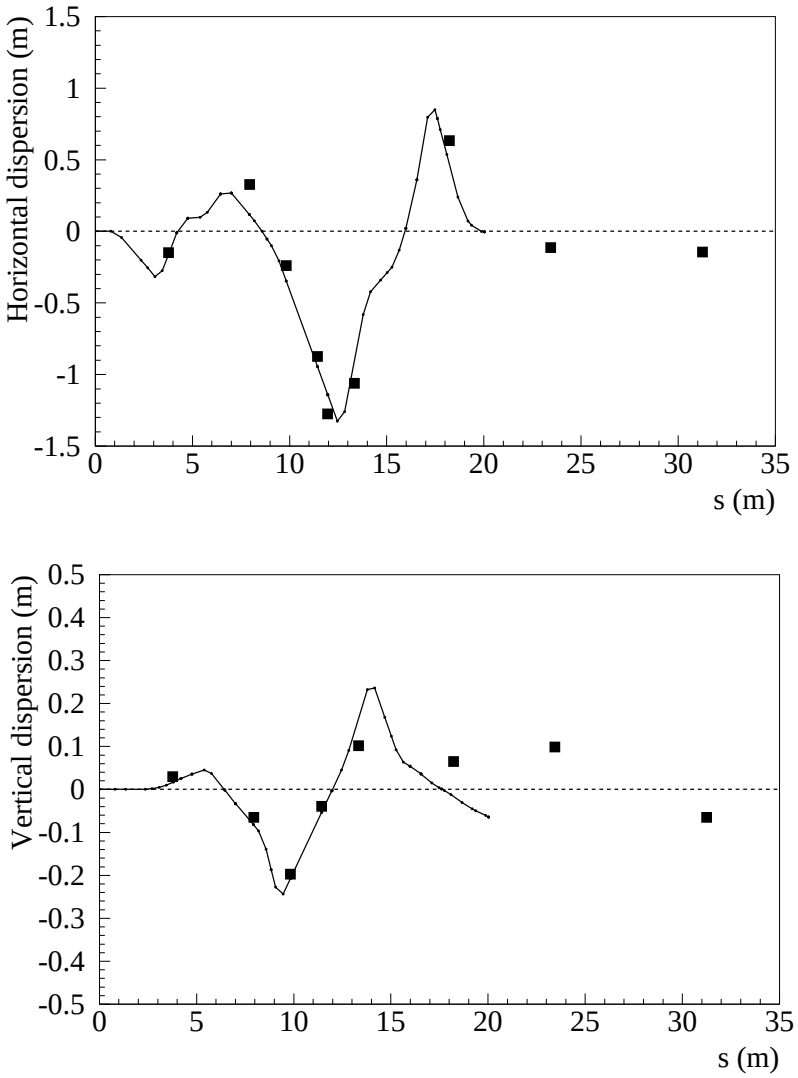

Figure 9: Horizontal and vertical dispersion, as measured along the following sequence: HIE.MTV01, HIE.UMA21, HIE.UMA22, HIE.UMA23, HIE.MTV23, HIE.MSH23 (not for the vertical dispersion), HIE.MTV30, HR.UMA83, HR.UMA91. The dispersion curves predicted with MAD in the HIE line are also shown.

The results obtained in the injection line are very consistent with our previous dispersion measurements [3]: there is a good agreement with the MAD simulations in the horizontal plane, but there is also a discrepancy between the measured and expected values of the vertical dispersion in HIE.MTV30. However, when changing the current in HIE.QDW24 from 90 to 95 A in the MAD simulations, it becomes possible to obtain a good agreement with the measured value. In the ring injection region (corresponding to the two points on the right-hand side of the previous plots), our measurements show that both the horizontal and vertical dispersions are close to zero, as required for a matched injection into the isochronous ring.

6.3 Tune measurements in the isochronous ring

During the previous operation period, we have shown that tune measurements could be performed in the isochronous ring with a method based on a Fourier Transform analysis of the horizontal and vertical beam position monitors signals after injection [3]. In August 2002, we measured the horizontal and vertical tunes for various settings and we have compared them with the results from MAD simulations. Figure 10 shows that there is a very good agreement between the expected and measured values.

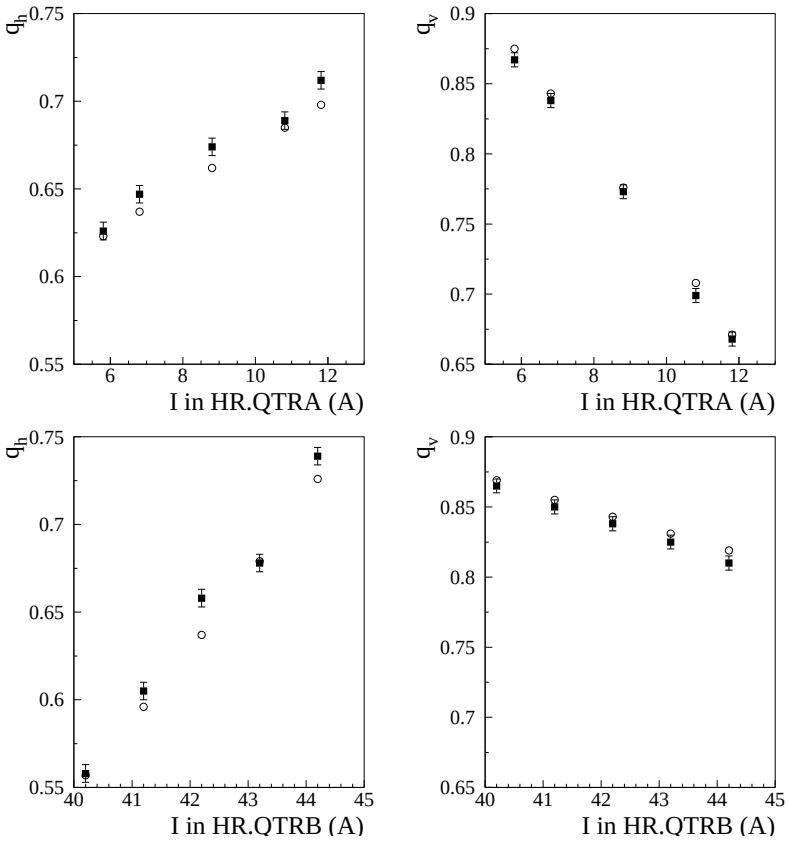

Figure 10: Fractional part of the horizontal and vertical tunes as a function of the current in HR.QTRA and HR.QTRB: the open circles correspond to the tune calculated with MAD, while the full squares correspond to the experimental values (the error bars show the uncertainty on the peak position measurement in the frequency spectrum). The integer value of the horizontal (resp. vertical) tune is 4 (resp. 3) in all cases.

6.4 Isochronicity measurements

During the last week of this operation period, we performed isochronicity measurements with the streak camera in the EPA ring.

In a first step, we took a streak camera image of the whole pulse after 5 turns in the ring, as shown in Figure 11. The intra-pulse beamloading is clearly visible, i.e. the energy is slightly higher for the bunches in the head of the pulse than for the bunches in the tail. Each bunch travelling through the accelerating structures withdraws some energy from the RF field, hence the first bunches of the pulse experience a higher acceleration than the bunches arriving later.

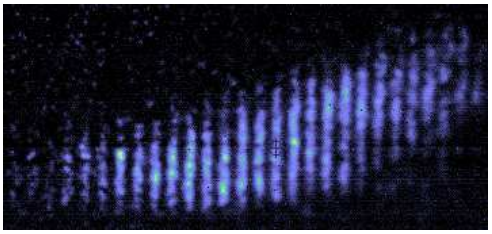

Figure 11: Streak camera image of the whole electron pulse. The horizontal axis represents time, while the vertical axis represents a position which is related to the beam energy. The intra-pulse beamloading is clearly visible: the bunches in the head (right-hand side) and the tail (left-hand side) of the pulse have different energies.

We looked at different regions of one electron pulse, by tuning the delay of the streak camera acquisition system. When doing this, we could notice that the energy-time correlation was also different for the bunches in the head, the middle or the tail of the pulse. Because of the energy variation along the pulse, second order isochronicity effects become visible and they result in different energy-time correlations in different parts of the pulse. This second order isochronicity effect is likely to be produced in the injection line, where no sextupole is installed. Figure 12 shows three streak camera images, which have been taken with different delays, after 10 turns in the ring. They clearly show that both the energy and the energy-time correlation change along the pulse.

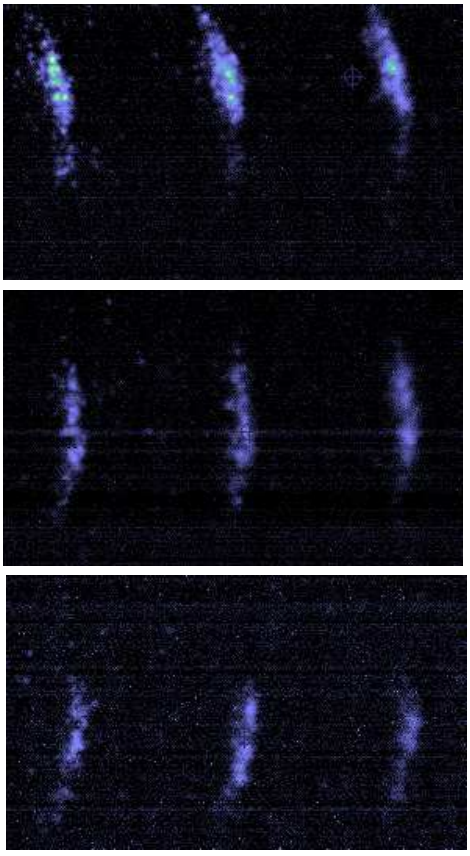

Figure 12: Streak camera images of three electron bunches: the delay was tuned in order to observe the head, the middle and the tail of the pulse (from top to bottom).

Due to the bunch to bunch energy variation, a non-isochronous ring optics would also lead to a change in distance between these bunches. We measured the bunch spacing in one pulse at the first turn and also after 5, 10, 20, 40 and 60 turns in the ring. Figure 13 shows that the bunch spacing is independent of the number of turns made by the pulse in the ring, which confirms that it is indeed isochronous.

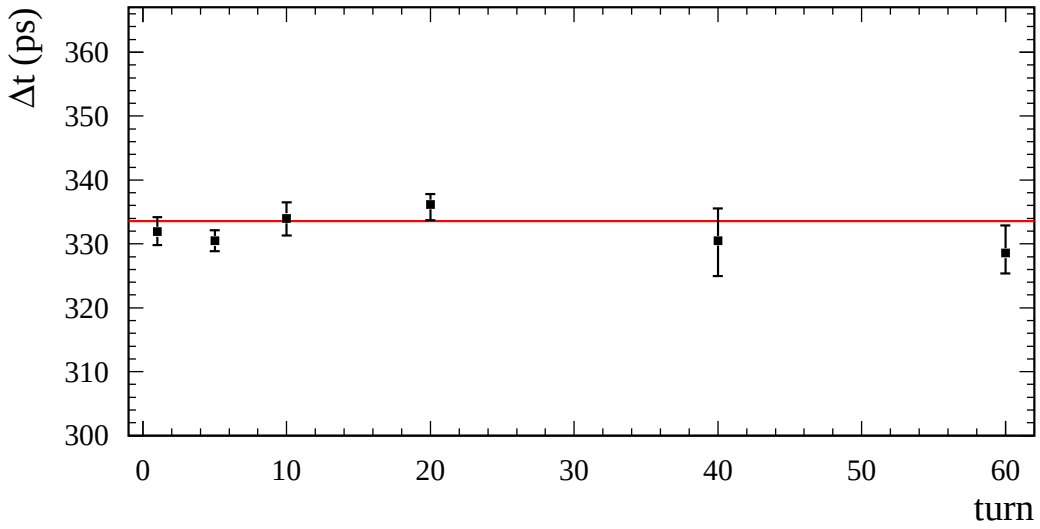

Figure 13: Bunch spacing measured with the streak camera at various turns of the pulse in the ring. The reference (solid line) corresponds to the nominal bunch spacing at 2.998550 GHz. The error bars show the variations measured over eight images in one streak camera shot.

7 Conclusion

In this note, we reported on the operation of the CTF3 Preliminary Phase between May 27 and August 23, 2002. In June, the first demonstration of the bunch frequency multiplication was performed, first at half the nominal energy and with two bunch trains only, then at the nominal energy with factors four and five. During the summer 2002, additional measurements confirmed the very good agreement between the experimental and simulated lattice.

In this operation period, the procedure used to combine the bunch trains was not checked in details and more investigations are needed in order to minimize losses and optimize, among others, the timing of the injected bunches with respect to the RF deflecting field, or to accurately monitor the bunch frequency multiplication. New RF deflectors with a larger aperture, built by INFN Frascati, and a phase monitor, designed by Uppsala University, were installed in CTF3 between August 26 and September 16. We will report on the new measurements related to the bunch frequency multiplication in a future note.

Acknowledgements

The research of A. Ferrari has been supported by a Marie Curie Fellowship of the European Community Programme ”Improving Human Research Potentiel and the Socio-economic Knowledge Base” under contract number HPMF-CT-2000-00865.

References

[1] R. Corsini, A. Ferrari, L. Rinolfi, T. Risselada, P. Royer, F. Tecker, ”Beam Dynamics for the CTF3 Preliminary Phase”, CLIC note 470.

[2] R. Corsini, B. Dupuy, A. Ferrari, L. Rinolfi, P. Royer and F. Tecker, ”Commissioning of the CLIC Test Facility 3 Preliminary Phase in 2001”, CERN-PS-2002-005 (AE), CLIC note 507.

[3] R. Corsini, A. Ferrari, L. Rinolfi, P. Royer and F. Tecker, ”Report on the operation of the CTF3 Preliminary Phase, 8 April - 24 May 2002”, PS/AE note 2002-141, CTF3 note 049.